RSC Advances

PAPER

View Article Online
View Journal | View Issue



Cite this: *RSC Adv.*, 2017, **7**, 42634

# Orange phosphor $Li_2SrSiON_2:Eu^{2+}$ for blue light chip based warm white LEDs†

Aijun Mao,[abc] Zhengyan Zhao[abc] and Yuhua Wang *[abc]

Received 26th June 2017
Accepted 21st August 2017

DOI: 10.1039/c7ra07085c

rsc.li/rsc-advances

Oxynitride $Li_2SrSiON_2$ was synthesized by introducing $N^{3-}$ into the $Li_2SrSiO_4$ lattice, which is suitable for $Eu^{2+}$ doping. It crystallizes in an trigonal structure with the space group of $P3_121$ (152) and cell parameter $a = b = 5.0131(0)$ Å, $c = 12.4270(1)$ Å and $V = 270.46$ Å$^3$. Under blue light (450 nm) excitation, the representative sample $Li_2Sr_{0.98}SiON_2:0.02Eu^{2+}$ exhibits a bright broad band orange emission peaking at 586 nm with an external quantum efficiency of 52.7%. Its emission intensity at 150 °C remained 78% of that measured at 25 °C. Warm white light-emitting diode 1 (W-LED1) was prepared by combining a blue LED chip and LSSON:$0.02Eu^{2+}$. High color rendering index ($R_a \sim 90$) warm W-LED2 was fabricated by combing a blue light chip, $BaSi_2O_2N_2:Eu^{2+}$, and $Li_2Sr_{0.98}SiON_2:0.02Eu^{2+}$. The chromaticity coordinate and correlated color temperature (CCT) of W-LED2 are (0.3625, 0.3539) and ~4386 K, respectively. Excellent optical properties allow it to be an attractive orange phosphor for warm W-LEDs.

## 1. Instruction

White light-emitting diodes (W-LEDs) have been regarded as the next generation light source because of their low power consumption, high brightness, high efficiency, longer life, and environmental friendliness.[1–3] Although UV/NUV pumped chips with a phosphor blend of RGB-emitting phosphors can obtain white light with tunable color temperature and high color rendering, and it is very easy to obtain UV/NUV light excited blue/green/red phosphors in $Ce^{3+}/Eu^{2+}$ doped compounds, the poor efficiency of the UV/NUV LED chips and re-absorption of different phosphors have been commonly encountered. In addition, UV/NUV light is harmful to human skin and eyes.[4–6] Therefore, blue light chip excited W-LEDs are considered as healthier, energy-saving, and environmentally friendly lighting sources.[7–10] A mature production route is the combination of blue light chip and yellow phosphor $(Y,Gd)_3(Al,Ga)_5O_{12}:Ce^{3+}$ (YAG:$Ce^{3+}$). While low color rendering index ($R_a \sim 75$) and high correlated color temperature (CCT ~ 7000 K) are presented in this combination due to insufficiency of red component in the spectrum. These characteristics resulting in limited application areas, such as indoor lighting, commercial lighting, *etc.* Two main schemes have been developed to fabricate W-LEDs containing sufficient red component: one is optical properties improvement of YAG phosphor *via* composition variation.[11–13] And the other is adding red nitride phosphor ($M_2Si_5N_8:Eu^{2+}$,Sr$[LiAl_3N_4]:Eu^{2+}$ or $CaAlSiN_3:Eu^{2+}$) into the combination of blue chip and YAG phosphor.[7,14–16] In principle, the combination of blue light chip and orange phosphor (contain sufficient red component) is the most direct method to obtain warm white light.[17–19] Moreover, incorporation with green phosphors can significantly improve rendering color index ($R_a$). Although efficient green phosphors suitable for blue light chip have been realized in $Eu^{2+}$ doped oxynitridosilicates: $MSi_2O_2N_2:Eu^{2+}$ (M = Ca, Sr, Ba),[20] M-α/β-SiAlON:$Eu^{2+}$ (M = Mg, Ca, Sr, Ba), efficient orange conversion under blue light excitation is still scarce at present,[21,22] which still needs to involve more effort. Nitridation of $Ce^{3+}/Eu^{2+}$ doped oxides, and the oxydation of $Ce^{3+}/Eu^{2+}$ doped nitrides should be the primary consideration.

For activator ions $Ce^{3+}/Eu^{2+}$, their 5d electrons unshielded from the crystal field by the 5s and 5p electrons when in the excited state, the spectra properties are strongly affected by the surrounding environment. Owing to $N^{3-}$ has a higher effective charge compared with $O^{2-}$, and Pauling's electron negativity of N (3.04) is smaller than that of O (3.50).[19–22] Coordinating with $N^{3-}$ would cause a stronger nephelauxetic effect and bigger crystal field splitting. When $N^{3-}$ was introduced into $Ce^{3+}/Eu^{2+}$ doped oxide, wavelength of emission peak generally takes place red-movement.[8] Moreover, most of the pure nitride phosphors have excellent thermal stability owing to their structure framework consisted of rigid $[SiN_4]$ tetrahedrals. At present, pure silicon nitride phosphors are synthesized in a critical condition with expensive raw materials. While $Li_2SiN_2:Eu^{3+}$ is an exception,[23] which was synthesized at 900 °C, as mild as oxide counterparts.[24–27] So novel lithium-containing oxynitride

[a]*Department of Materials Science, School of Physical Science and Technology, Lanzhou University, Lanzhou, China. E-mail: wyh@lzu.edu.cn; Fax: +86-931-8913554; Tel: +86-931-8912772*

[b]*Key Laboratory for Special Function Materials and Structural Design of the Ministry of Education, Lanzhou, China*

[c]*National & Local Joint Engineering Laboratory for Optical Conversion Materials and Technology, Lanzhou University, Lanzhou, 730000, China*

† Electronic supplementary information (ESI) available. See DOI: 10.1039/c7ra07085c

phosphors can be synthesized in a mild condition by introducing N into oxide phosphors. Among lithium-containing oxide phosphors, $Li_2SrSiO_4$:$Eu^{2+}$ was reported to an intensely yellow phosphor peaking at 570 nm.[26,27] Shortage of its luminescence properties are insufficient red component in spectrum and weak thermal stability, indicating that it to be a good target for nitridation.

Based on above investigation, $Eu^{2+}$ doped oxynitride luminescence materials with chemical compositions ($Li_2Sr_{1-x}SiON_2$:$xEu^{2+}$) LSSON:$xEu^{2+}$ were designed and synthesized. Crystal structure of host LSSON were studied. Photo-luminescence (PL) properties of representative sample were investigated systemically. In addition, W-LEDs have been fabricated and the corresponding electroluminescence (EL) properties were measured to evaluate its application performance. As expected, representative sample LSSON:$Eu^{2+}$ can serve as an attractive orange phosphor for blue light chip based warm W-LEDs.

## 2. Materials and synthesis

Powder samples $Li_2Sr_{1-x}SiON_2$:$xEu^{2+}$ were synthesized by using stoichiometric amounts of raw materials of $Li_2CO_3$ (A.R), $SrCO_3$ (A.R), $SiO_2$ (A.R), $Si_3N_4$ (A.R) and $Eu_2O_3$ (A.R). Excess of $Li_2CO_3$ (3 wt%) was added, because $Li_2CO_3$ is easy to volatilize at high temperature, causing large number of vacancies in host and weaken luminescence efficient of $Eu^{2+}$ ion. Meantime, $Li_2CO_3$ could also act as a co-solvent to improve the crystallinity of samples. The mixture was placed in a ceramic crucible and fired at 800 °C (with a heating rate of 5 °C $min^{-1}$) for 4 h, then cooling down to 500 °C (with a cooling rate of 5 °C $min^{-1}$). Whole sintering process was conducted in a reductive atmosphere of 90/10 (volume) $N_2/NH_3$.

## 3. Characterization

Phase purity was confirmed by X-ray power diffraction (XRD) on a Rigaku D/Max-2400 X-ray diffractometer using Ni-filtered Cu Kα radiation. Rietveld refinement was performed by using General Structure Analysis System (GSAS) package. The sample morphology was examined by using scanning electron microscopy (SEM; Hitachi S-4800). Element composition and microstructure were measured on a FEI Tecnai 35 F30 transmission electron microscopy (TEM, FEI Tecnai F30, operated at 300 kV) equipped with an energy dispersive X-ray spectroscopy (EDX). Internal ($\eta_i$) quantum efficiencies (QE) was calculated by using the following eqn (1):[28]

$$\eta_i = \frac{\int \lambda P(\lambda) d\lambda}{\int \lambda [E(\lambda) - R(\lambda)] d\lambda} \quad (1)$$

where $E(\lambda)/h\nu$, $R(\lambda)/h\nu$, and $P(\lambda)/h\nu$ are the numbers of photons in the spectrum of excitation, reflectance, and emission, respectively. Room-temperature and temperature-dependent PL spectra were recorded on a FLS-920T fluorescence spectrophotometer with a 450 W Xe lamp for excitation and a standard TAP-02 to control the temperature. The diffuse reflectance spectra (DRS) were measured on PE lambda 950 UV-vis spectrophotometer by using $Ba_2SiO_4$ power as the reference. PL decay curves were measured with a FLS-920T fluorescence spectrophotometer with a F900 ns (μF900 microsecond) flash lamp used as the light source. W-LED1 was prepared by using blue light chip (~450 nm, P/N 046VB-S-FA1) and as-prepared LSSON:0.02$Eu^{2+}$. W-LED2 was prepared by using blue light chip, $BaSi_2O_2N_2$:$Eu^{2+}$ and LSSON:0.02$Eu^{2+}$. EL spectra, $R_a$ values, CCT, and Commission Internationale de l'Eclairage (CIE) chromaticity coordinates were measured using a SphereOptics integrating sphere with LED measurement starter packages.

## 4. Results and discussion

### 4.1 Phase identification and morphology observation

To confirm phase-pure $Li_2SrSiON_2$ solid solution is the optimal host, Rietveld refinement was conducted based on single crystal data of $Li_2SrSiO_4$ (ICSD-167334). The experimental, calculated, and difference results of Rietveld refinement are given in ESI Fig. S1.† A exact match was yielded by refining atomic positions, temperature-dependent factor and profile parameters. Refined crystallographic data was listed in ESI Tables S1 and S2,† respectively. Information in Table S2† shows that the $N^{3-}$ ion content is about 67 percent of all anions. Corresponding cell parameters are $a = b = 5.0131(0)$ Å, $c = 12.4270(1)$ Å and $V = 270.46$ Å$^3$, which are smaller than that of $Li_2SrSiO_4$: $a = b = 5.0228(0)$ Å, $c = 12.4552(1)$ Å and $V = 272.13$ Å$^3$. Reason of lattice contract is that $N^{3-}$ ionic radii is smaller than $O^{2-}$. SEM observation in Fig. 1a shows that $Li_2SrSiO_{4-1.5z}N_z$ powers have a good dispersibility. TEM image in Fig. 1b gives the selected grain with ideal morphology. EDX spectrum in Fig. 1c reveals that chemical compositions of the selected grain are Sr, Si, O, N. And no impurity elements exist. Li is not included due to it belongs to the light element and can not be detected by the TEM detector. Quantitative analyses using EDX showed that $N^{3-}/O^{2-}$ ions ratio basically match with the refined ratio in Table S2† (about 67%), indicating that designed compound can be written as $Li_2SrSiON_2$ (LSSON). Inter-planar spacing in Fig. 1d was measured to be ~0.5013 nm, match with refined inter planar distance (100) and (010). In ESI Fig. S2,† no detectable XRD peaks corresponding to impurities exist in the XRD spectra of LSSON:$xEu^{2+}$ solid solutions, indicating that single phase solid solutions were obtained. Owing to radius of $Eu^{2+}$ [$R = 1.25$ Å, CN = 8] is close to $Sr^{2+}$ [$R = 1.26$, CN = 8], peak location has no obvious shift with the increase of $Eu^{2+}$ ion concentration.

There is a structure overview of LSSON lattice presented in Fig. 2, along the [100] direction (Fig. 2a), a condensed crystal networks structurally built upon three dimensional $Si(O,N)_4$ tetrahedrons layers interleaving connection to $Li(O,N)_4$ tetrahedrons layers. $Sr^{2+}$ residing in triangle voids (60%) and quadrangle voids (40%). Viewed along [100] and [201], rigid framework of crystal cell (Fig. 2b and c) consists of orderly edge-shared $Li(O,N)_4$ tetrahedrals and corner-shared $Si(O,N)_4$ tetrahedrals. All $Sr^{2+}$ coordinated by six $O^{2-}$ and two $N^{3-}$, and reside in the 3c site, as shown in Fig. 2d. Mean Sr–O/N bond length is about 2.481Å, and mean $Sr^{2+}$ – $Sr^{2+}$ distance is about 5.014 Å. It is also noticed that $N_2$ located around $Sr^{2+}$, while $N_1$ located near $Li^+$ and $Si^{4+}$. $Eu^{2+}$ is

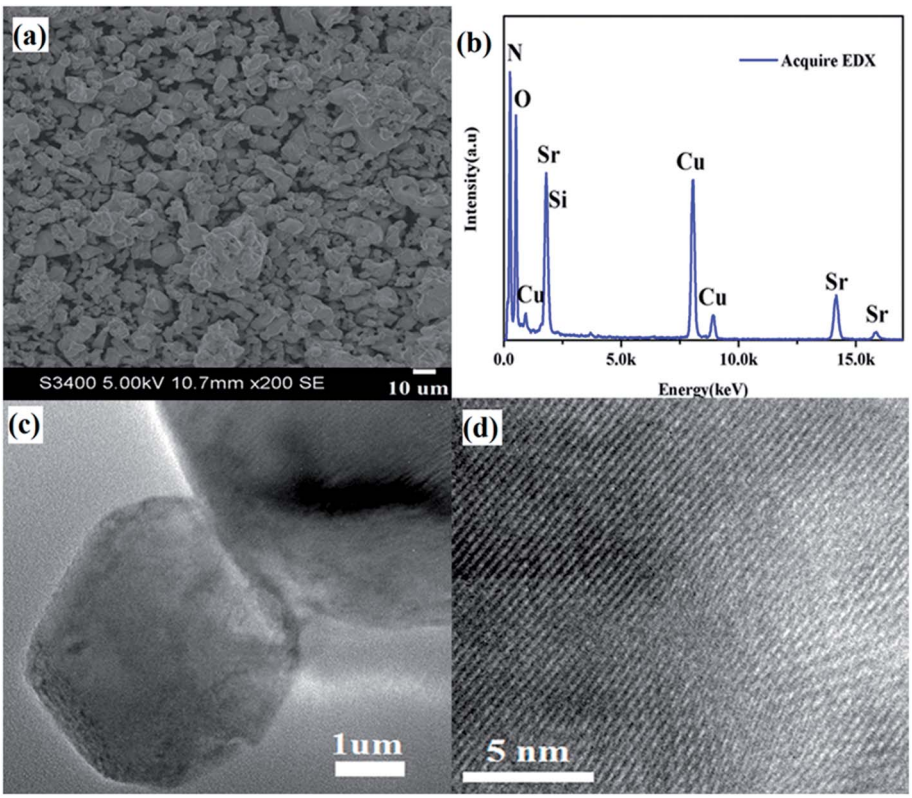


Fig. 1 (a) SEM image, (b) EDX spectrum, (c) TEM image, (d) HRTEM image of LSSON.

expected to replace $Sr^{2+}$, as the ions radii of $Eu^{2+}$ (1.25 Å) and $Sr^{2+}$ (1.26 Å) are almost identical.[29] To support that one crystallographic site of $Eu^{2+}$ in LSSON, decay curve of LSSON:0.02$Eu^{2+}$ excited at 450 nm and monitored at 586 nm was measured which given in ESI Fig. S3.† Thus, it can be well fitted by single exponential eqn (2), indicating that only one crystallographic site of $Eu^{2+}$ existed in the process of decay.[30]

$$I = I_0 \exp(-t/\tau) \quad (2)$$

where $I$ and $I_0$ are the luminescence intensity; $t$ is time; and $\tau$ is the lifetime for the exponential component. The efficient decay

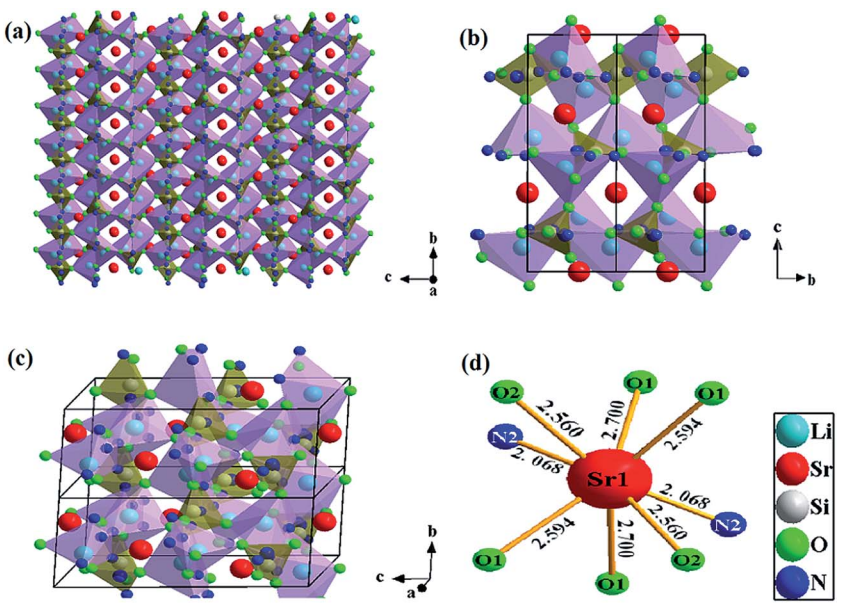


Fig. 2 Structure overview of LSSON lattice viewed along (a) and (b) [100] and (c) [201], (d) coordination environments of Sr site.

time ($\tau$) can be obtained by the following eqn (3). And the lifetime of $Eu^{2+}$ ions in LSSON:0.02$Eu^{2+}$ was calculated to be 1.051 μs. It falls in the range of radiative lifetime of $Eu^{2+}$ ion in most hosts (0.2–2.0 μs):[31,32]

$$\tau = \frac{\int_0^\infty tI(t)\mathrm{d}t}{\int_0^\infty I(t)\mathrm{d}t} \quad (3)$$

### 4.2 Optical properties

Optical properties of LSSON:$Eu^{2+}$ are showed in Fig. 3, including UV-visible DRS, PL(E) spectra, and EL spectra of self-packaged W-LEDs. In Fig. 3a, an absorption band in the range of 200–300 nm is observed in DRS of un-doped LSSON, which comes from the optical band gap of LSSON. For LSSON:0.02$Eu^{2+}$ with orange body color, two absorption bands present in the spectrum range of 200–300 and 300–500 nm, respectively. First one ascribe to the optical band gap of LSSON. While the second one assign to the 4f → 5d transition of $Eu^{2+}$, and correspond to its PLE spectrum.

PL spectra of LSSON:$x$$Eu^{2+}$ ($0.01 \leqq x \leqq 0.04$) under 450 nm excitation are showed in Fig. 3b. All of emission spectra cover a wide spectra region ranging from 550 nm to 700 nm. As $Eu^{2+}$ ions content increased, luminescence intensity was increasing and reached a maximum at $x = 0.02$. Then concentration quenching phenomenon occurred caused by non-radiative energy transfer between activator ions.[33] The optimal sample

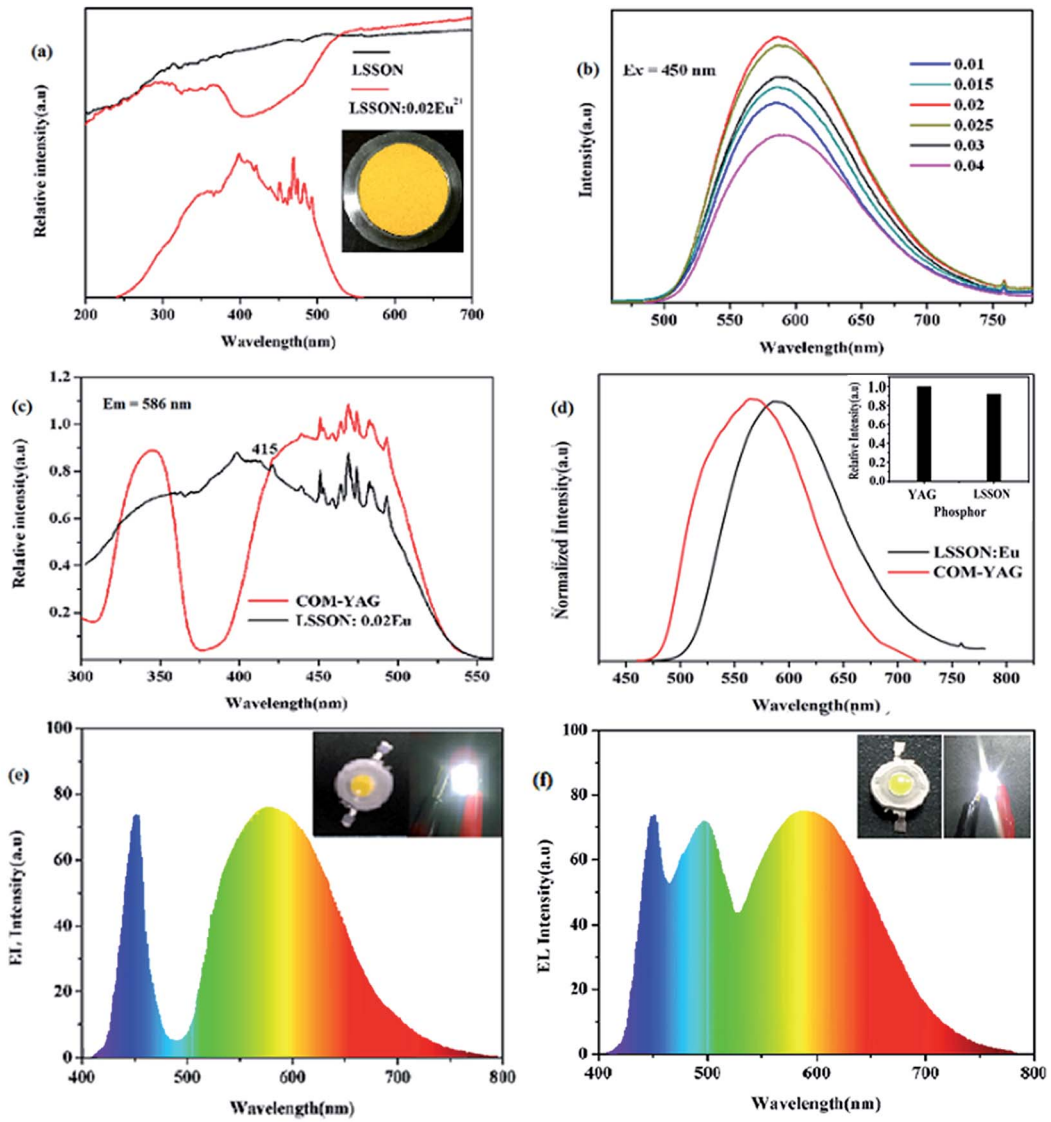


Fig. 3 (a) DRS of LSSON and LSSON:0.02$Eu^{2+}$, together with excitation spectrum and body color of LSSON:0.02$Eu^{2+}$ (b) emission spectra of LSSON:$x$$Eu^{2+}$ ($0.01 \leqq x \leqq 0.04$) with various $Eu^{2+}$ concentration under 450 nm excitation. Comparison of (c) excitation (monitored at 586 nm) and (d) emission (excited at 450 nm) spectra of LSSON:0.02$Eu^{2+}$ and commercial YAG:$Ce^{3+}$ (YAG04, Intematix). (e) EL spectrum of W-LED1 composed of blue LED chip (~450 nm, P/N 046VB-S-FA1) and LSSON:0.02$Eu^{2+}$, (f) EL spectrum of W-LED2 composed of blue LED chip (~450 nm, P/N 046VB-S-FA1), $BaSi_2O_2N_2$:$Eu^{2+}$ and LSSON:0.02$Eu^{2+}$.

LSSON:0.02$Eu^{2+}$ exhibits a bright orange emission peaking at 586 nm with a wide full-width at half-maximum (~110 nm) and an external quantum efficiency of 52.7%. In addition, the emission peak position was redshifted from 585 nm to 588 nm as the $Eu^{2+}$ ion concentration increases (ESI Fig. S4a†). Generally, there are two possible reasons for the redshift: one is the increased crystal field splitting of $Eu^{2+}$ ion. The other is re-absorption. In our case, the shrink of single cell can be ignored as $Eu^{2+}$ concentration increases, as well as the change of bond length, co-valency, and symmetry. Therefore, the increase of crystal field splitting can be ignored. Red-shift of emission peak should be ascribed to re-absorption.

To validate this deduction, critical distance ($R_c$) between $Eu^{2+}$ of non-radiative energy transfer need to be estimated. Blasse proved that $R_c$ has relationship with critical concentration of activator ions, as shown in eqn (4):[34]

$$R_c = 2\left[\frac{3V}{4\pi X_c N}\right]^{\frac{1}{3}} \quad (4)$$

where $V$ is the unit cell volume, $N$ is the number of $Eu^{2+}$ sites per unit cell, and $X_c$ is the critical concentration of $Eu^{2+}$. $R_c$ was calculated to be 20.51 Å by using parameter values: $V$ = 270.59(0) $Å^3$, $X_c$ = 0.02, $N$ = 3, which much bigger than the measured $Sr^{2+}$–$Sr^{2+}$ distance, indicating that non-radiative energy transfer can be easy to happen and quenching concentration are small ($X_c = 0.02$). Together with small overlap between PLE and PL spectra, energy transfer mechanism could be dominated by electrostatic interaction, and estimated by eqn (5):[34]

$$I/x = K[1 + \beta(x)^{\theta/3}] - 1 \quad (5)$$

where $I$ is the emission intensity, $x$ is the activator ions concentration, $K$ and $\beta$ are constants in a given host, $\theta$ is an indication of electric multipolar character with $\theta$ = 6, 8, 10 corresponding to dipole–dipole, dipole–quadrupole, or quadrupole–quadrupole interactions, respectively. In ESI Fig. S4b,† the emission intensity ($I$) and corresponding $Eu^{2+}$ ion concentration are linear fitted. The slope [log($I/x$)/log($x$)] is about $-1.735 = -(\theta/3) \approx -2$, and $\theta$ value is close to 6. So concentration quenching mechanism is dominated by dipole–dipole interaction.

Comparison between LSSON:0.02$Eu^{2+}$ and commercial YAG:$Ce^{3+}$ (YAG04, Intematix) are shown in Fig. 3c and d. PLE spectrum of LSSON:0.02$Eu^{2+}$ is obviously wider than YAG:$Ce^{3+}$. Under 450 nm excitation, its PL intensity is about 92% of that of YAG:$Ce^{3+}$. More importantly, its emission spectrum contains more red component than YAG:$Ce^{3+}$, which is highly desirable for high quality warm white light applications. To further evaluate application performance of phosphor LSSON:0.02$Eu^{2+}$, W-LED1 was prepared by combining

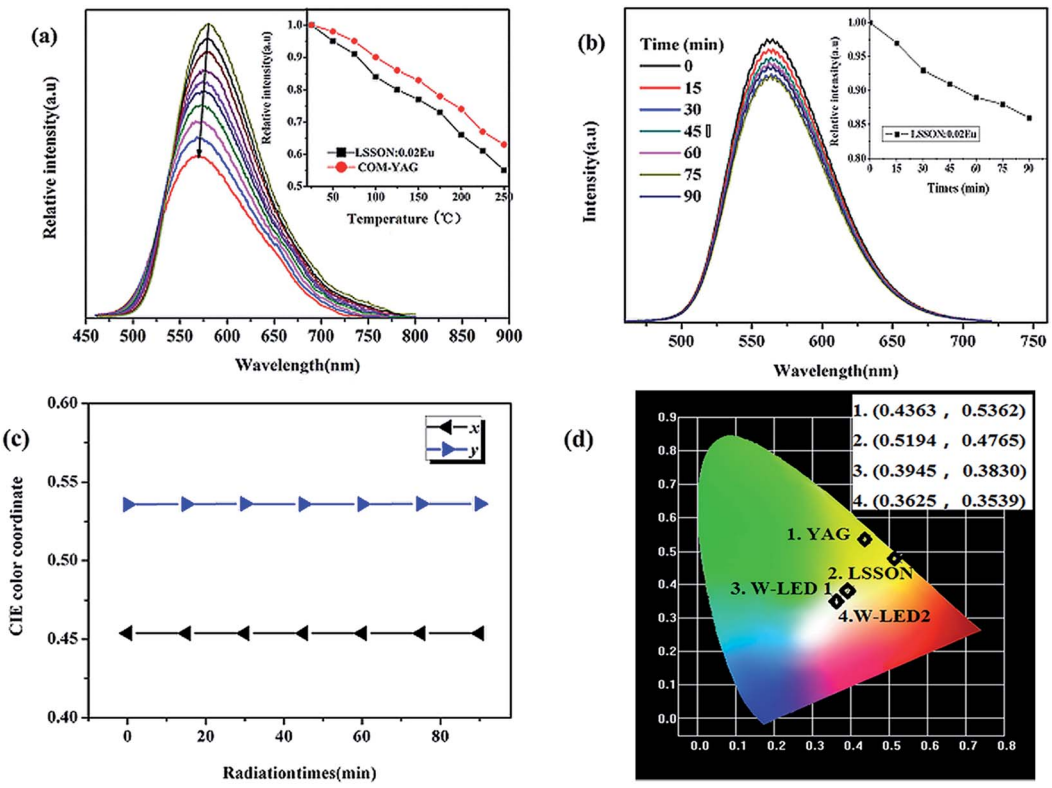


Fig. 4 (a) Temperature dependence of PL spectra of LSSON:0.02$Eu^{2+}$excited at 450 nm. The inset shows PL intensity variation of LSSON:0.02$Eu^{2+}$ and YAG:$Ce^{3+}$ as a function of temperature. (b) CL spectra (insets show the dependence of the emission intensity of LSSON:0.02$Eu^{2+}$ on time) (c) CIE coordinates of LSSON:0.02$Eu^{2+}$ phosphor as a function of probe current under 5 kV voltage and 50 mA filament current. (d) Chromaticity coordinates of LSSON:0.02$Eu^{2+}$ and commercial YAG:$Ce^{3+}$. And CIE chromaticity of emission from W-LEDs.

 

blue LED chip and LSSON:0.02$Eu^{2+}$. Its EL spectrum driven by 300 mA current was measured, as shown in Fig. 3e. The corresponding CIE chromaticity, CCT, and $R_a$ were calculated to be (0.3945, 0.383), 3687 K, and 71, respectively. W-LED1 exhibits warm white light, while color rendering index $R_a$ < 75 owing to lack of blue-green component (470–520 nm). Then W-LED2 was prepared by combining blue LED chip, $BaSi_2O_2N_2$:$Eu^{2+}$ and LSSON:0.02$Eu^{2+}$. Its EL spectrum also driven by 300 mA current [Fig. 3f]. The corresponding CIE chromaticity, CCT, and $R_a$ were calculated to be (0.3625, 0.3539), 4386 K, and ~90, respectively. Those parameters demonstrate that sample LSSON:0.02$Eu^{2+}$ can be used in warm W-LEDs for indoor lighting.

Heat, generated in LED chip, generally reaches ~150 °C. Thus the thermal stability is a key parameter of a phosphor used in LEDs. Temperature dependent PL spectra of LSSON:0.02$Eu^{2+}$ under 450 nm excitation are shown in Fig. 4a. In addition, comparison of thermal stability between LSSON:0.02$Eu^{2+}$ and YAG:$Ce^{3+}$ was conducted. With rising of temperatures, blue-shift of emission peak can be observed, which ascribed to thermally active phonon-assisted tunneling from excited states of lower-energy emission band to those of higher energy emission band.[34] Meanwhile, emission intensity is gradually decreasing, which caused by thermally activated cross-over from the $4f^6$5d-excited state to the $4f^7$ ground state. By increasing temperature up to 150 °C, emission intensity remain at 78% of that measured at room temperature. LSSON:0.02$Eu^{2+}$ has good thermal stability and better than the reported orange phosphors.[17,18,33] Good thermal stability generally correspond to rigid lattice. Then degradation behavior of LSSON:0.02$Eu^{2+}$ were measured to evaluate its structure stability [Fig. 4b]. Under high energy electron beam continuous excitation (5 kV), emission peak remain stable through the whole excitation progress. Emission intensity remain 88% of that measured at the beginning after continuous electrons excitation for 90 min (inserted figure). The CIE coordination in Fig. 4c is nearly unchanged. Above results reveal that LSSON:0.02$Eu^{2+}$ has stable lattice.

The activation energy for thermal quenching can be estimated by following eqn (6):[35]

$$I(T) = \frac{I_0}{1 + A\exp\left(\frac{-\Delta E}{K_B T}\right)} \quad (6)$$

where $I_0$ is the initial intensity, $I(T)$ is the intensity at $T$ °C, $A$ is a constant, $\Delta E$ is the activation energy for thermal quenching, and $K_B$ is the Boltzmann's constant. As calculated in Fig. S4,† $\Delta E$ for LSSON:0.02$Eu^{2+}$ and YAG:$Ce^{3+}$ are 0.2185 eV and 0.2663 eV, respectively. Activation energy $\Delta E$ of YAG:$Ce^{3+}$ is higher than that of LSSON:0.02$Eu^{2+}$. This result indicates YAG:$Ce^{3+}$ has a better thermal stability.[36] At last, the calculated CIE color coordinates were used to characterize the emission of LSSON:0.02$Eu^{2+}$, YAG:$Ce^{3+}$, and W-LEDs [see in Fig. 4d]. Under 450 nm excitation, chromaticity coordinates of LSSON:0.02$Eu^{2+}$ and YAG:$Ce^{3+}$ are (0.5194, 0.4765) and (0.4363, 0.5362),respectively. Larger $x$ value correspond to more red component. Chromaticity coordinates of W-LED1 and W-LED2 are (0.3945, 0.383) and (0.3625, 0.3539), respectively. They both locate in the warm white zone.

## 5. Conclusion

Oxynitride host LSSON for $Eu^{2+}$ doping was synthesized by using $N^{3-}$ partially substitute for $O^{2-}$ in $Li_2SrSiO_4$ lattice. Its rigid framework consists of edge-shared $Li(O,N)_4$ tetrahedrals and corner-shared $Si(O,N)_4$ tetrahedrals. Under 450 nm excitation, LSSON:0.02 $Eu^{2+}$ exhibits a intense broad band orange emission peaking at 586 nm and with CIE coordinate of (0,5194, 0,4765). Emission intensity remain at 78% at 150 °C of that measured at room temperature. High color rendering index ($R_a$ ~ 90) warm W-LED was syntesized by combing of blue LED chip, $BaSi_2O_2N_2$:$Eu^{2+}$ and LSSON:0.02$Eu^{2+}$. Corresponding chromaticity coordinates and CCT are (0.3625, 0.3539) and 4386 K, respectively. Above results indicate that the synthesized LSSON:0.02$Eu^{2+}$ can be used as an orange phosphor for blue light chip based warm W-LEDs.

## Conflicts of interest

There are no conflicts to declare.

## Acknowledgements

This work is supported by the National Natural Science Funds of China (Grant no. 51372105), and the Gansu Province development and reform 181 commission (NDRC) no. 2013,1336, National Natural Science Foundation of China (51502122).

## References

1 Nobelprize.org. Nobel Media AB 2014, "The Nobel Prize in Physics 2014", 2014.
2 W. Y. Huang, F. Yoshimura, K. Ueda, Y. Shimomura, H. S. Sheu, T. S. Chan, C. Y. Chiang, W. Z. Zhou and R. S. Liu, *Chem. Mater.*, 2014, **26**, 2075–2085.
3 W. Y. Huang, F. Yoshimura, K. Ueda, Y. Shimomura, H. S. Sheu, T. S. Chan, H. F. Greer, W. Zhou, S. F. Hu, R. S. Liu and J. P. Attfield, *Angew. Chem., Int. Ed.*, 2013, **52**, 8260–8264.
4 H. J. Song, D. K. Yim, H. S. Roh, I. S. Cho, S. J. Kim, Y. H. Jin, H. W. Shim, D. W. Kim and K. S. Hong, *J. Mater. Chem. C*, 2013, **1**, 500.
5 S. P. Lee, C. H. Huang, T. S. Chan and T. M. Chen, *ACS Appl. Mater. Interfaces*, 2014, **6**, 7260–7267.
6 Z. G. Xia, J. Q. Zhuang and L. B. Liao, *Inorg. Chem.*, 2012, **51**, 7202–7209.
7 R. J. Xie and N. Hirosaki, *Adv. Mater.*, 2007, **8**, 588–600.
8 Z. Y. Zhao, Z. G. Yang, Y. R. Shi, C. Wang, B. T. Liu, G. Zhu and Y. H. Wang, *J. Mater. Chem. C*, 2013, **1**, 1407–1412.
9 H. M. Zhu, C. C. Lin, W. Q. Luo, S. T. Shu, Z. G. Liu, Y. S. Liu, J. T. Kong, E. Ma, Y. C. Cao, R. S. Liu and X. Y. Chen, *Nat. Commun.*, 2014, **4312**, 891–896.

10 P. Pust, V. Weiler, C. Hech, A. Tücks, A. S. Wochnik, A. K. Hen, D. Wiechert, C. Scheu, P. J. Schmidt and W. Schnick, *Nat. Mater.*, 2014, **13**, 891–896.
11 L. Chen, X. L. Chen, F. Y. Liu, H. H. Chen, H. Wang, E. L. Zhao, Y. Jiang, T. S. Chan, C. H. Wang, W. H. Zhang, Y. Wang and S. F. Chen, *Sci. Rep.*, 2015, **5**, 1–17.
12 M. Raukas, K. K. Bergenek, G. C. Wel, N. M. Zink and S. Lange, *US* patent 2012/0018673 A1, 2012.
13 I. G. Chen, Y. T. Nien, H. J. Lu and C. W. Ma, *US* Patent: US 9,085,733 B2, 2015.
14 P. Pust, V. Weiler, C. Hecht, *et al.*, *Nat. Mater.*, 2014, **13**, 891–896.
15 M. Zeuner, F. Hintze and W. Schnick, *Chem. Mater.*, 2008, **21**, 336–342.
16 M. Fujinaga, T. Ueda, T. Sakai and S. Jida, *US* Patent:US9,023,240,B2, 2015.
17 W. B. Park, S. P. Singh, C. Yoon and K. S. Sohn, *J. Mater. Chem. C*, 2013, **1**, 1832–1839.
18 Q. Q. Zhu, L. Wang, N. Hirosaki, L. Y. Hao, X. Xu and R. J. Xie, *Chem. Mater.*, 2016, **28**, 4829–4839.
19 K. Horky and W. Schnick, *Chem. Mater.*, 2017, **10**, 5–13.
20 V. Bachmann, C. Ronda, O. Oeckler, W. Schnick and A. Meijerink, *Chem. Mater.*, 2009, **21**, 316–325.
21 J. H. Ryu, H. S. Won, Y.-G. Park, S. H. Kim, W. Y. Song, H. Suzuki, C.-B. Yoon, D. H. Kim, W. J. Park and C. Yoon, *Electrochem. Solid-State Lett.*, 2010, **13**, H30–H32.
22 Y. F. Kargin, N. S. Akhmadullina, A. S. Lysenkov, A. A. Ashmarin, A. V. Ishchnko, L. V. Viktorov, O. S. Teslenko, B. V. Shul'gin and A. V. Spirina, *Inorg. Mater.*, 2012, **48**, 827–831.
23 J. Y. Ding, Y. Y. Li, Q. S. Wu, Q. Long, C. Wang and Y. H. Wang, *J. Mater. Chem. C*, 2015, **3**, 8542–8549.
24 L. H. Jiang, Y. L. Zhang, C. Y. Li, J. Q. Hao and Q. Su, *Mater. Lett.*, 2007, **61**, 5107–5109.
25 H. Yu, D. G. Deng, S. Q. Xu, C. P. Yu, H. Y. Yin and Q. L. Nie, *J. Lumin.*, 2012, **132**, 2553–2556.
26 C. Kulshreshtha, A. K. Sharma and K. S. Soh, *J. Electrochem. Soc.*, 2009, **156**, J52–J56.
27 M. P. Saradhi and U. V. Varadaraju, *Chem. Mater.*, 2006, **18**, 5267–5272.
28 P. P. Dai, C. Li, X. T. Zhang, J. Xu, X. Chen, X. L. Wang, Y. Jia, X. J. Wang and Y. C. Liu, *Light: Sci. Appl.*, 2016, **5**, 16024.
29 J. Y. Han, W. B. Im, G. Y. Lee and D. Y. Jeon, *J. Mater. Chem.*, 2012, **22**, 8793–8798.
30 Y. H. Kim, P. Arunkumar, B. Y. Kim, S. Unithrattil, E. Kim, S. H. Moon, J. Y. Hyun, K. H. Kim, D. Lee, J. S. Lee and W. B. Im, *Nat. Mater.*, 2017, **16**, 543–550.
31 J. Zhou, Z. G. Xia, M. X. Yang and K. Shen, *J. Mater. Chem.*, 2012, **22**, 21935.
32 L. Wang, X. J. Wang, T. Takeda, N. Hirosaki, Y. T. Tsai, R. S. Liu and R. J. Xie, *Chem. Mater.*, 2015, **27**, 8457–8466.
33 P. Dorenbos, *J. Phys.: Condens. Matter*, 2005, **17**, 8103–8110.
34 W. Z. Sun, Y. L. Jia, R. Pang, H. F. Li, T. F. Ma, D. Li, J. P. Fu, S. Zhang, L. H. Jiang and C. Y. Li, *ACS Appl. Mater. Interfaces*, 2015, **7**, 25219–25226.
35 H. Liu, L. Chen, X. F. Zhou, R. H. Liu and W. D. Zhuang, *J. Solid State Chem.*, 2017, **246**, 145–149.
36 Q. Y. Shao, Y. Dong, J. Q. Jiang, C. Liang and J. H. He, *J. Lumin.*, 2011, **131**, 1013–1015.